Myeloid STAT3 promotes formation of colitis-associated colorectal cancer in mice

(Article begins on next page)

27 August 2024

UNIVERSITÀ DEGLI STUDI DI TORINO

Myeloid STAT3 promotes formation of colitis-associated colorectal
cancer

Myeloid STAT3 promotes formation of colitis-associated colorectal cancer

Pathria P[1], Gotthardt D[2], Prchal-Murphy M[2], Putz EM[2], Holcmann M[1], Schlederer M[3], Grabner B[3], Crncec I[1], Svinka J[1], Musteanu M[4], Hoffmann T[5], Filipits M[1], Berger W[1], Poli V[6], Kenner L[3], Bilban M[7], Casanova E[3], Müller M[8], Strobl B[8], Bayer E[1], Mohr, T[1], Sexl V[2], Eferl R[1*]

[1]Medical University Vienna & Comprehensive Cancer Center (CCC), Institute for Cancer Research, Vienna, Austria

[2]Institute for Pharmacology and Toxicology, University of Veterinary Medicine Vienna, Austria

[3]Ludwig Boltzmann Institute for Cancer Research LBICR, Vienna, Austria

[4]Spanish National Cancer Research Centre (CNIO), Madrid, Spain

[5]Institute of Molecular Pathology IMP, Vienna, Austria

[6]Department of Genetics, Biology and Biochemistry, University of Turin, Italy

[7]Medical University Vienna, Department of Medical and Chemical Laboratory Diagnostics, Vienna, Austria

[8]Institute of Animal Breeding and Genetics, University of Veterinary Medicine Vienna, Austria

*corresponding author

Phone: +43 1 40160-57571

Fax: +43 1 40160-957510

E-Mail: robert.eferl@meduniwien.ac.at

Abstract

Myeloid cells crosstalk with T cells and prevent anti-tumor T cell responses in a STAT3-dependent manner. We investigated the role of STAT3 in myeloid stromal cells of murine autochthonous colorectal cancers (CRCs). Conditional ablation of STAT3 in myeloid cells (STAT3$^{\Delta M}$) strongly suppressed formation of Azoxymethane/Dextransulfate (AOM/DSS-induced CRCs. Tumors that succeeded to develop in STAT3$^{\Delta M}$ mice displayed enhanced stromalization with altered composition of stromal immune cells. Transplantation of MC38 tumor cells into STAT3$^{\Delta M}$ host mice indicated that growth of CRCs was preferentially controlled by aberrant T cell activities. Gene expression profiling of autochthonous STAT3$^{\Delta M}$ CRCs demonstrated that aberrant T cell activation was maintained in the tumor stroma and not suppressed by tumor derived factors. Moreover, STAT3$^{\Delta M}$ CRCs displayed profound activation of STAT3, Myc and TGFß signaling in tumor cells whereas NFκB/p65 signaling was compromised. These tumor cell-autonomous molecular changes might contribute to editing and immune escape of CRCs. Therefore, targeting these pathways could improve the efficacy of immune therapies and prevent relapse of escaped cancers.

Introduction

Colorectal cancer (CRC) represents the third most common form of cancer in humans worldwide. Major mutations leading to CRC formation have been identified in genes for adenomatous polyposis coli (Apc), K-ras, components of the TGFß signalling pathway (Smad4 or TGFßRII) and p53[1]. CRCs develop frequently in the context of inflammatory bowel disease demonstrating a tumor-promoting role of inflammation[2]. Moreover, a robust infiltration of T cells, B cells, neutrophils, dentritic cells (DCs), natural killer cells (NKs), tumor-associated macrophages (TAMs) and myeloid derived suppressor cells (MDSCs) is observed in the CRC tumor stroma[2]. Stromal immune cells support growth of CRC via production of cytokines that activate the oncogenic transcription factors NFκB and STAT3[3]. Moreover, the stroma contains immune cells with anti-tumor activities which force tumors to develop mechanisms of escape and immune suppression[4]. One paradigm is the ability of tumors to modulate polarization of TAMs. Bacterial LPS and the Th1 cytokine IFNγ polarize macrophages towards the classical M1 phenotype which is responsible for innate immune attack of infectious pathogens but also neoplastic cells. Alternative activation by Th2 cytokines IL4 and IL13 polarizes macrophages towards the M2 phenotype which is characterized by low expression of M1 markers (IL12, iNos) but high expression of M2 markers (IL10, VEGF, matrix metalloproteases, IL1decoyR, Arginase-1, CCL17, CCL22)[5, 6]. M2 macrophages have reduced anti-tumorigenic activities but are considered to promote angiogenesis and tumor progression[5, 6]. Repolarization of M2 macrophages towards the M1 phenotype represents a promising option for stromal anti-tumor therapies which was recently demonstrated in a mouse model for glioblastoma[7]. Another layer of complexity was recently discovered in breast tumors where an additional TAM population, distinguishably from M1 or M2 polarized macrophages, was identified[8].

STAT3 phosphorylation at tyrosine residue 705 (pY-STAT3) via Janus kinases (JAKs) is induced by pro- and anti-inflammatory cytokines such as IL6, IL10, IL11, IL21 and IL23[9]. The oncogenic role of STAT3 in CRC tumor cells has been demonstrated in several studies[10-13]. However, STAT3 seems to have a tumor-suppressive role in advanced CRCs because Apc^{Min} mice lacking STAT3 in tumor cells developed aggressive intestinal carcinomas that were not observed in Apc^{Min} control animals[14-16]. STAT3 promotes CRC formation via regulation of genes implicated in cell survival and cell proliferation[17, 18] and modulates nuclear localization of ß-Catenin by post-transcriptional mechanisms[16, 19]. In addition, STAT3 activation represents an important immune escape mechanism as cancer cells exploit STAT3-induced expression of VEGF and IL10 to blunt maturation of stromal DCs. An immune suppressive action is further given by the STAT3 dependent repression of pro-inflammatory cytokines and chemokines including IFNγ, TNFα, IL6 and IP10[20, 21].

Apart from tumor-cell specific functions, STAT3 is considered to promote tumor formation when being activated in stromal cells of CRCs[16, 17, 22]. STAT3 activation is the result of cytokines produced by both, stromal and tumor cells. Thereby a reciprocal feedback loop between tumor cells and stromal cells is established that maintains STAT3 activation in both cellular compartments[21]. Tumor transplantation experiments into host mice lacking STAT3 in the hematopoietic system demonstrated that STAT3 activation in immune cells prevents anti-tumorigenic activities of DCs, Th1 cells, NKs and neutrophils[23]. This led to the concept of inhibiting stromal/hematopoietic STAT3 as potential strategy for cancer immunotherapy[24]. Myeloid STAT3 is considered of particular importance for the modulation of Th1-like anti-tumor responses[25]. STAT3 directly regulates the expression of the pro-tumorigenic cytokine IL23 whereas production of the Th1 cytokine IL12 by dentritic cells is suppressed via an indirect NFκB-dependent mechanism[26]. Consequently, inhibition of STAT3 in myeloid cells and B cells using CpG-STAT3 siRNA enhanced cytotoxic T cell (CTL)-mediated responses in a melanoma transplantation model[27].

Here we demonstrate that ablation of myeloid STAT3 significantly interfered with development of autochthonous AOM/DSS-induced colorectal tumors in mice. This effect was mediated by an enhanced anti-tumor T cell response. Weighted gene correlation network analysis of STAT3$^{\Delta M}$ tumor and stroma tissue uncovered sustained T cell-mediated immune surveillance in escaped tumors which was accompanied by deregulation of several inflammatory signaling pathways in tumors cells. The latter might be part of a signaling network that contributes to immune editing which implicates that targeting of these pathways could synergistically improve the efficacy of immune therapies.

Results

Myeloid STAT3 promotes formation of colorectal tumors

We investigated the role of STAT3 in the myeloid stromal cells of autochthonous colorectal tumors developing under inflammatory conditions. For this purpose, we used mice with conditional inactivation of STAT3 in myeloid cells (STAT3$^{\Delta M}$ = LysM$^{Cre/Cre}$ STAT3$^{flox/flox}$) and corresponding controls (STAT3^{wt} = LysM$^{Cre/Cre}$ STAT3$^{+/+}$). Successful deletion of STAT3 in myeloid cells was confirmed by Western blot analysis in granulocyte-macrophage precursors differentiated from bone marrow cells in vitro and FACS-sorted peritoneal macrophages (Supplementary Figure 1a) as well as by qPCR analysis of FACS-sorted splenic macrophages (Supplementary Figure 1b). Histopathological analysis and IHC-staining revealed no major changes of cell differentiation or proliferation in colon and small intestine of STAT3$^{\Delta M}$ mice except for a slight reduction of enteroendocrine cell numbers (Supplementary Figure 2a). Deletion of STAT3 in myeloid cells provokes Th1 differentiation and development of colitis[28, 29]. However, we failed to detect severe colitis in STAT3$^{\Delta M}$ mice using histopathology and IHC-staining for macrophages and T cells in the C57BL/6 genetic background used (Supplementary Figure 2b). However, flow cytometric analysis of colonic lamina propria immune cells from STAT3$^{\Delta M}$ mice after short term challenge with DSS uncovered a consistently increased mean fluorescence intensity of the activating protein CD69 on CD4^{+} T cells (Supplementary Figure 3) which is associated with Th1 differentiation[30].

To investigate the impact of myeloid STAT3 in autochthonous tumors, we induced colorectal cancer in STAT3^{wt} and STAT3$^{\Delta M}$ mice using the Azoxymethan/Dextransulfate (AOM/DSS) protocol (Figure 1a). Tumor formation was significantly impaired in STAT3$^{\Delta M}$ mice (Figure 1b). The numbers of tumor nodules detectable was reduced irrespective of the gender whereas the mean tumor area was only reduced in female STAT3$^{\Delta M}$ mice (Figure 1b). For all further analysis, CRCs from male STAT3$^{\Delta M}$ mice were investigated. Tumor parameters such as cell proliferation and cell survival were not significantly altered in STAT3$^{\Delta M}$ CRCs (Figure 1c). However, we found increased numbers of blood vessels in the tumor stroma (Figure 1d). These data indicate that STAT3 in myeloid cells promotes formation of AOM/DSS-induced CRCs by mechanisms distinct from proliferation or apoptosis.

Myeloid STAT3 regulates stromal composition of CRCs

Tumor progression depends on the reciprocal crosstalk between tumor and stroma cells. Remarkably, histopathologic and immunohistochemical examination revealed an increased stromalization of STAT3$^{\Delta M}$ CRCs when compared with STAT3^{wt} CRCs (Figure 2a). Although increased stromalization is frequently associated with tumor progression and enhanced

invasiveness, no significant alteration in the percentages of low grade tumors, high grade tumors and carcinomas was observed in STAT3$^{\Delta M}$ mice (Figure 2d).

Within the tumor stroma the immune cell composition differed in STAT3$^{\Delta M}$ CRCs. The percentages of Gr1$^+$ granulocytes and FoxP3$^+$ regulatory T cells were reduced whereas neutrophilic esterase$^+$ neutrophils, RORγt$^+$ Th17 cells and toluidine blue-stained mast cells were almost absent. In contrast, CD45R$^+$ B cells were found at higher numbers (Figure 2b; Supplementary Figure 4). Interestingly, NKp46$^+$ NK cells accumulated preferentially at the margin of STAT3$^{\Delta M}$ CRCs (Supplementary Figure 4h). Consistent with a role of STAT3 in polarization of macrophages we found a reduction of cells expressing the M2 protein Arginase-1 paralleled by an increase in the number of M1 expressing iNOS-positive cells (Figure 2c). The percentages of stromal cells expressing NK proteins NKG2A and NKG2D as well as cells expressing the cytotoxic factor Granzyme B (cytotoxic T cells and granulocytes) was not significantly altered in the stroma of STAT3$^{\Delta M}$ CRCs (Figure 2c). These data indicate that STAT3 in myeloid cells determines the cellular composition of the CRC tumor stroma.

Myeloid STAT3 is not required for NK cell-mediated immune surveillance of CRCs

Loss of STAT3 in myeloid cells leads to an aberrant activation of NK and T cells[23, 31]. Thus, we studied whether reduced tumorigenesis is due to an improved immune surveillance exerted by NK and T cells. NK cell-dependent cytotoxicity was assessed in vitro using spleen-derived NK cells and CFSE-stained Yac-1 target cells. No significant differences in killing efficacies of NK cells isolated from STAT3^{wt} or STAT3$^{\Delta M}$ mice were detected (Figure 3a). Similarly, numbers of CD3$^-$ NK1.1$^+$ DX5$^+$ NKp46$^+$ NK cells in the spleen and the expression of NK cell maturation markers (CD27, KLRG-1) were unchanged (Supplementary Figure 5a) as were the percentages of NKG2D$^+$, NKG2A/C/E$^+$, DNAM-1$^+$ and Ly49C/I$^+$ NK cells (Supplementary Figure 5b). We detected only one consistent change: the number of NK cells expressing the activating receptor Ly49D, which recognizes MHC class I alloantigens, was reduced in STAT3$^{\Delta M}$ mice (Figure 3b) whereas the mean fluorescence intensity of the activating receptor NKG2D (but not NKGD2A/C/E) was increased (Figure 3c). As NKG2D is an important receptor for the recognition of stress-induced ligands on tumors, we performed transplantation experiments with isogenic C57BL/6-derived p185 leukemia cells that are eradicated by NK cell-mediated mechanisms. Although p185-derived tumors were slightly smaller in STAT3$^{\Delta M}$ host animals, indicative for an improved NK cell-mediated tumor surveillance, the differences did not reach statistical significance (Figure 3d).

We next investigated the impact of NK cell-mediated immune surveillance on formation of autochthonous CRCs. For that purpose, we treated STAT5^{wt} and STAT5$^{\Delta NK}$ mice with AOM/DSS. STAT5$^{\Delta NK}$ mice represent a model for genetic ablation of NK cell functions[32]. No significant increase in AOM/DSS-induced tumor formation was observed in STAT5$^{\Delta NK}$ mice

despite of a substantial reduction of NKp46$^+$ cell numbers in the gut (Figure 3e). These data suggest that NK cell-mediated killing activities do not significantly contribute to immune surveillance of AOM/DSS-induced CRCs.

Myeloid STAT3 is required for T cell-mediated immune surveillance of CRCs

Apart from NK cells, cytotoxic T cells (CTLs) and helper T cell functions are key determinants for tumor immune surveillance. In particular for human CRCs, it has been demonstrated that stromal T cell infiltration correlates with better prognosis[33]. Therefore, we performed in vivo cytotoxicity assays in STAT3^{wt} and STAT3$^{\Delta M}$ mice. m-TRP2$_{181-188}$-immunized STAT3$^{\Delta M}$ mice displayed a slight but significantly enhanced killing activity of m-TRP2$_{181-188}$-pulsed CFSE-labeled splenocytes in vivo (Figure 4a) indicating enhanced cytotoxic T cell activity in STAT3$^{\Delta M}$ mice even in the absence of tumors. To address whether the enhanced T cell-dependent cytotoxicity extends to CRCs, we transplanted isogenic colorectal MC38 cancer cells into STAT3^{wt} and STAT3$^{\Delta M}$ hosts. Remarkably, tumor growth was significantly impaired in STAT3$^{\Delta M}$ host animals (Figure 4b). Reduced tumor growth was accompanied by higher numbers of CD4$^+$ T cells but only slightly increased numbers of CD8$^+$ cytotoxic T lymphocytes in tumor lysates (Figure 4c). However, the percentages of CD4$^+$ or CD8$^+$ T cells co-expressing the activation marker CD69 were similar in STAT3^{wt} and STAT3$^{\Delta M}$ hosts (data not shown). The number of GR1^{hi} CD11b$^+$ MDSCs was also elevated in tumors of STAT3$^{\Delta M}$ host mice whereas GR1^{lo} CD11b$^+$ CD11c^{lo} tumor-associated macrophages were reduced (Figure 4c). MDSCs can provide a costimulatory signal for T cell activation and survival through expression of CD80, a ligand for CD28. Indeed, higher numbers of GR1^{hi} CD11b$^+$ CD80$^+$ MDSCs were present in MC38 tumors of STAT3$^{\Delta M}$ hosts (data not shown). No changes in NK cell infiltration and only a slightly increased expression of NKG2D on infiltrating NK cells were observed (Figure 4c and data not shown). Moreover, Rael and MHCI protein expression levels were similar on MC38 tumor cells (data not shown). These data indicate that growth of colorectal cancer cells is preferentially limited by T cell-mediated antitumor immunity.

CRCs of STAT3$^{\Delta M}$ mice escape T cell-mediated killing

In order to molecularly characterize immune-mediated mechanisms in AOM/DSS-induced CRCs, microarray gene expression profiling was performed with RNA samples from microdissected tumor and stroma tissue of paraffin-embedded and formalin-fixed tissues. Microarray data of the stroma tissues were subjected to weighted gene correlation network analysis (WGCNA). Modules of high correlation for genes implicated in immune responses, cytokine production and angiogenesis were identified (Supplementary Figure 6). The latter correlated with the increased density of blood vessels observed in the stroma of STAT3$^{\Delta M}$

tumors (Figure 1d). However, network plots revealed no clear deregulation of individual angiogenesis pathways suggesting that blood vessel formation is promoted by a complex molecular mechanism (Supplementary Figure 7). In contrast, network plots for GO terms in immune modules revealed a clear result with massive upregulation of corresponding genes in the stroma of STAT3[ΔM] tumors (Figure 5). A "T cell activation" network plot demonstrated a strong correlation between dock2/ptpn6/thy1 and dock2/CD48/tnfrsf4 expression. Moreover, upregulation of cytokine/chemokine receptors, MHC class II molecules and complement factors was identified in "T cell activation", "adaptive immune response", "innate immune response" and "positive regulation of immune response" network plots (Figure 5a). Corresponding network plots for response and production of cytokines demonstrated correlations between Irg1/IL-1ß/Cxcl10 and Irg1/IL-1ß/Hilpda expression (Figure 5b). These results suggest a strong enhancement of immune responses that are particularly related to T cell activation. Consistently, genes belonging to the Immunologic Constant of Rejection (ICR) signature[34] and genes indicative for T cell activation were upregulated in the stroma of STAT3[ΔM] CRCs (Supplementary Figure 9a, b). Interestingly, expression of PD-L1 and PD-L2, two ligands that antagonize T cell activities, were also upregulated (Supplementary Figure 9b) which might represent an adaptive response to limit T cell activation. These data suggest that AOM/DSS-induced CRCs in STAT3[ΔM] mice are under control of T cell-mediated immune surveillance which leads to reduced tumor numbers.

Cell-autonomous changes of putative immunoediting pathways in STAT3[ΔM] CRCs
Remarkably, the enhanced stromal T cell activation had no impact on the size of AOM/DSS-induced STAT3[ΔM] tumors at least in male mice (Figure 1b). This indicates that CRCs develop strategies to escape the strong immunogenic environment in STAT3[ΔM] mice. Therefore, we investigated microarray expression data, obtained with microdissected tumor cell tissue, for molecular processes indicative for immunoediting. RNA expression of immunosuppressive tumor-derived factors (Supplementary Figure 9c) and NKG2D stress-induced ligands (Supplementary Figure 9d) was not significantly altered in STAT3[ΔM] CRCs. Protein expression of the NKGD2 ligand H60, as assessed by IHC, was not detectable in STAT3[wt] and STAT3[ΔM] CRCs (data not shown). Moreover, protein expression of Rael was not significantly reduced in cancer cells of STAT3[ΔM] mice (data not shown) excluding selective immunoediting for Rael^{low} CRCs in order to escape NK cell killing. Interestingly, STAT3[ΔM] CRCs contained increased numbers of stromal CD45R^{+} B cells (Figure 2b) and complement factors were upregulated (Figure 5, "adaptive immune response"). However, expression of mCRPs, which protect tumor cells from complement attack, was not differentially regulated in STAT3[wt] and STAT3[ΔM] CRCs (Supplementary Figure 9e). These data indicate that no

selective immunoediting for mCRP[high] CRCs in order to escape complement-mediated tumor killing has occurred.

Little is known about signaling pathways in tumor cells that promote immune escape but a positive role has been attributed to STAT3. Therefore, we used the Molecular Signature Database of the Broad Institute for identification of differentially regulated signaling pathways. Overlap analysis of genes upregulated in STAT3$^{\Delta M}$ tumor cells (>2-fold) with curated gene sets identified "fevr_ctnnb1_targets_up" and "zheng_IL22_signaling_up" as most significant candidates. These gene sets represents genes that are upregulated in intestinal crypt cells upon deletion of ß-catenin[35] and genes upregulated in colonic tissue after treatment with IL22 (a potent inducer of STAT3 activity)[36], respectively. This indicated that Wnt signaling was compromised and STAT3 signaling was aberrantly activated in STAT3$^{\Delta M}$ tumor cells. However, IHC analysis revealed no significant reduction of ß-Catenin-positive tumor cells in STAT3$^{\Delta M}$ mice (Supplementary Figure 8). Remarkably, levels of STAT3 and activated STAT3 (pY-STAT3) were significantly elevated in STAT3$^{\Delta M}$ tumor cells (Figure 6a).

Overlap analysis of genes downregulated in STAT3$^{\Delta M}$ tumor cells (>2-fold) identified "karlsson_tgfß1_targets_dn", "phong_tnf_response_via_p38_partial" and again several gene sets implicated in Wnt signaling with "sansom_wnt_pathway_require_myc" as most significant candidate. The latter is derived from a study demonstrating that Myc regulates most Wnt target genes in the small intestine[37]. This suggests that we identified Wnt signaling gene sets in the absence of ß-Catenin deregulation because of aberrant Myc expression. Consistent with this hypothesis, Myc expression was increased in STAT3$^{\Delta M}$ tumor cells (Figure 6b). The "karlsson_tgfß1_targets_dn" and "phong_tnf_response_via_p38_partial" gene sets represent genes downregulated by TGFß1 in MEFs[38] and genes that are activated by TNFα in Calu-6 lung cancer cells[39], respectively. This data indicated that TGFß signaling was aberrantly activated whereas NFκB signaling was compromised in STAT3$^{\Delta M}$ tumor cells. Consistently, levels of the p65 NFκB subunit were reduced in STAT3$^{\Delta M}$ tumor cells (Figure 6c). Moreover, pSmad2 levels were increased in STAT3$^{\Delta M}$ tumor cells (Figure 6d) which correlated with increased numbers of TGFß-producing cells in the tumor stroma (Figure 6e). In summary, these data suggest that STAT3$^{\Delta M}$ CRCs have established a signaling network that contributes to tumor immune escape.

Discussion

Macrophages with disruption of STAT3 signaling have a constitutively activated phenotype and are capable of restoring the tumor responsiveness of tolerant T cells suggesting an important implication for cancer immunotherapy[31]. The consequences of hematopoietic STAT3 targeting on augmentation of anti-tumor immune responses have been comprehensively studied in tumor cell transplantation models[20]. In contrast, the applicability of STAT3-based immunotherapy on autochthonous tumors is not well defined. It is also unclear if and through which molecular mechanisms autochthonous tumors adapt to STAT3-based immune surveillance. Targeting potential escape mechanisms might not only improve immunotherapy but also prevent tumor relapse. We describe for the first time that ablation of myeloid STAT3 interferes with development of autochthonous tumors in mice. The use of an autochthonous tumor model allowed us to investigate the cellular and molecular consequences of myeloid STAT3 ablation on stroma and tumor compartments. The data suggest that cross activation of anti-tumor T cell responses by STAT3-deficient myeloid cells cannot be efficiently suppressed by tumor-derived factors in colitis-associated CRCs. However, tumor cells seem to employ intrinsic molecular mechanisms to escape the strong immunogenic microenvironment in Stat3$^{\Delta M}$ mice.

Two types of inflammation have been described: "Bad inflammation" is characterized by the presence of Th2 cells, MDSCs, Tregs and M2 polarized macrophages and represents a tumor-promoting condition. "Good inflammation" is characterized by the presence of Th1 cells, CTLs, DCs and M1 polarized macrophages which mount an anti-tumor immune attack[40, 41]. However, even "good inflammation" can promote cancer formation through the mutagenic action of reactive oxygen species (ROS), chronic tissue damage and regeneration[2]. Loss of STAT3 in hematopoietic cells including macrophages and DCs results in spontaneous gut inflammation but it is unclear if this condition promotes or prevents formation of colitis-associated CRCs[29, 42, 43]. Interestingly, we have not observed a severe spontaneous colitis phenotype in Stat3$^{\Delta M}$ mice which was also reflected by a normal life span and fertility of Stat3$^{\Delta M}$ mice. This might be due to the used C57/BL6 genetic background or an alternative composition of the intestinal microflora because enterocolitis is significantly improved in Stat3$^{\Delta M}$ mice by ablation of TLR4 signaling[28]. Moreover, Stat3$^{\Delta M}$ and Stat3^{wt} mice responded similarly to DSS with respect to the activation status of intestinal inflammatory cells and colitis score indicating that aberrant immune responses did not occur in Stat3$^{\Delta M}$ mice in the absence of tumors. This is consistent with the NK and T cell activation assays, performed without tumor challenge, and corroborated by published data[23]. Therefore, STAT3-deficient myeloid cells seem to selectively promote tumor immune surveillance without major effects on non-tumor related immune cell functions. Enhanced immune surveillance seems to rely on myeloid cross activation of T cell rather than NK cell activities

as demonstrated by p185 and MC38 cell transplantation studies. Similarly, AOM/DSS-induced Stat3$^{\Delta M}$ CRCs might be primarily eradicated by T cell responses. This is consistent with the presence of stromal gene expression signatures in Stat3$^{\Delta M}$ tumors that are indicative for T cell activation. NK cell activities seem to play a minor role in immune surveillance of AOM/DSS-induced CRCs because Stat3$^{\Delta M}$ tumors displayed no stromal gene expression signature indicative for NK cell-mediated cytotoxicity and did not show downregulation of NKG2D stress-induced protein ligands. Moreover, CRC formation was not promoted in STAT5$^{\Delta NK}$ mice which display reduced NK cell activities[32]. However, the intestine also contains an autonomous NK cell compartment distinct from conventional NK cells that could exert anti-tumor activities[44].

A strong intratumoral CTL infiltration was observed in the majority of patients with early-stage CRCs whereas patients with a low cytotoxic response evolved to late-stage disease[34]. Moreover, it has been demonstrated that CD3$^+$, CD8$^+$ and CD45RO$^+$ stromal T cell densities and their intratumoral locations (Immunoscore) represents a better prognostic marker than conventional TNM staging[45]. Additional determination of a core gene expression signature called ICR (Immunologic Constant of Rejection) including ifng, il12, tbx21, irf1, stat1, gzma, gzmb, prf1, cxcl9, cxcl10, ccl5, cx3cl1, ccl2, madcam1, icam1 and vcam1 genes can refine the accuracy of prognosis[34]. T cells were the most abundant stromal cell type in AOM/DSS-induced CRCs although number and distribution of CD3$^+$ and CD8$^+$ cells was not different in Stat3$^{\Delta M}$ and Stat3^{wt} mice. Despite the unchanged Immunoscore, Stat3$^{\Delta M}$ tumors displayed upregulation of several core ICR genes (irf1, stat1, cxcl9 and ccl5) indicating that these marker genes are predictive for good prognosis in mice and humans. Among these core genes is ccl5 which encodes for the chemokine RANTES. RANTES is produced by STAT3-deficient myeloid cells and has been identified as a chemokine that prevents T cell anergy in tumor immune surveillance[31]. The ICR signature of Stat3$^{\Delta M}$ tumors had, however, no impact on tumor grading. Similarly, Cox multivariate analysis demonstrated that the T and N stages of early-stage human CRCs did not significantly correlate with their Immunoscore albeit T and N stages of advanced CRCs did[34].

Remarkably, STAT3 in myeloid cells regulates the stromal composition of CRCs which might result in pleiotropic tumor-promoting or tumor-suppressive effects. The altered stromal composition of Stat3$^{\Delta M}$ CRCs is most likely due to an altered cytokine and chemokine milieu that leads to differential attraction of immune cells. Consistent with this hypothesis, expression of stem cell factor (SCF), which is the major chemoattractant for mast cells, was found downregulated in tumor and stroma compartments of Stat3$^{\Delta M}$ CRCs (data not shown). This explains the reduced number of mast cells which was also reflected by reduced expression of mast cell proteases mcpt1 and mcpt2 in the stroma of Stat3$^{\Delta M}$ CRCs (data not shown). Interestingly, reduced numbers of stromal mast cells and increased numbers of

stromal T cells favored prognosis of human CRCs patients[33]. This indicates a reciprocal correlation between stromal T cell activation and reduced mast cell numbers which was also observed in the stroma of Stat3$^{\Delta M}$ CRCs. Higher vessel density was an additional stromal change in Stat3$^{\Delta M}$ CRCs although they contained M1 polarized macrophages which don't support angiogenesis as efficient as M2 polarized macrophages. Moreover, it has been demonstrated that STAT3 activation in MDSCs and TAMs of transplanted B16 melanomas favors tumor angiogenesis via regulation of several pro- and anti-angiogenic factors including VEGF, bFGF, IL1ß, MMP9, CCL2 and CXCL2[46]. This controversy might be reconciled by WGCN analysis of the tumor stroma which did not reveal single factors that could explain increased vessel density in Stat3$^{\Delta M}$ CRCs. However, negative regulators of angiogenesis were predominantly downregulated and positive regulators were predominantly upregulated indicating that the altered cytokine milieu and distinct cellular immune cell composition in Stat3$^{\Delta M}$ CRCs might favor angiogenesis via pleiotropic effects.

According to the concept of immunoediting, transformed cells are initially eradicated by NK, NKT and T cell responses. Surviving cancer cells remain in equilibrium between tumor cell proliferation and eradication by T cell activities. Edited tumor cell, however, escape T cell attack through various mechanisms and establish primary growths[47]. It has been demonstrated that tumors in immune compromised mice are less edited and express tumor antigens that would lead to eradication in immune competent hosts. This experimental system has mainly been used to identify tumor antigens implicated in immune editing[47]. In contrast to immune compromised mice, CRCs in Stat3$^{\Delta M}$ mice face a strong immunogenic environment. The CRCs were unable to reshape their stroma towards a tumor-promoting immune cell composition by tumor derived factors. The sustained stromal immune activities might force Stat3$^{\Delta M}$ CRCs to develop tumor cell-autonomous strategies for immune escape apart from mere downregulation of tumor antigens. Therefore, we interpret the changes of STAT3, NFκB, Myc and SMAD signaling pathways in Stat3$^{\Delta M}$ CRCs as editing events essential for tumor cell survival. Among these pathways, the importance for STAT3 expression in tumor cells and its relevance for immune evasion is well documented[48, 49] and has been demonstrated for various cancers including glioblastoma[50, 51] and squamous cell carcinoma[52]. Activation of STAT3 in tumor cells inhibits expression of Th1 immune stimulatory molecules. In contrast, activation of NFκB induces expression of Th1 mediators[53]. Therefore, p65-expressing Stat3$^{\Delta M}$ CRCs might be counter selected, despite the tumor-promoting activity of NFκB, because of further augmentation of anti-tumor immune responses. Interestingly, many of the Th1 mediators induced by NFκB are repressed by STAT3[53]. Consequently, activation of STAT3 and simultaneous repression of NFκB in Stat3$^{\Delta M}$ CRCs could lead to escape of tumors that are immunologically inconspicuous because of their compromised cytokine secretory phenotypes.

STAT3 inhibitors are in clinical trials for various types of leukemias and solid cancers[54]. Our data suggest that inhibition of STAT3 in CRCs would interfere with immune evasion of tumor cells and simultaneously increase anti-tumor T cell activities in the stroma. Combinatorial therapies with STAT3 inhibitors and inhibitors for immune evasion pathways could have similar synergistic effect for prevention of tumor relapse after immunotherapy.

Acknowledgements

Methods

Mice and in vivo experiments

C57BL/6 STAT3$^{\Delta M}$ (= LysM$^{Cre/Cre}$ STAT3$^{flox/flox}$) and corresponding STAT3^{wt} control (= LysM$^{Cre/Cre}$ STAT3$^{+/+}$) mice[55, 56] were employed for tumor induction with AOM/DSS. The LysMCre knock-in alleles were kept homozygous to account for potential Cre or LysM knock-in effects. For tumor transplantation studies, 1×10^5 of p185 or 1×10^6 of MC38 cells were injected subcutaneously. Host mice were sacrificed and tumors were weighed and analysed by flow cytometry 11 days (p185) and 14 days (MC38) after tumor transplantation.

In vivo cytotoxicity was evaluated as described[57]. In brief, mice were immunized by subcutaneous injection of 0.1mg/mouse m-TRP2$_{181-188}$ (Bachem) in combination with the adjuvant CpG-ODN 1668. Seven days later control mice and immunized mice received syngeneic splenocytes labeled with three different concentrations of the intracellular dye carboxyfluorescein succinimidyl ester (CFSE): 2.5, 0.25 and 0.025µM. The CFSE^{high} population was pulsed with the relevant m-TRP2$_{181-188}$ (10µg/ml), the CFSE^{mid} population was pulsed with the irrelevant peptide m-SIINFEKL (Bachem; 10µg/ml) and the CFSE^{low} population remained untreated. All three differently pulsed CFSE$^+$ populations were mixed in a 1:1:1 ratio and approximately 3×10^7 cells were injected via the lateral tail veins of recipient STAT3^{wt} and STAT3$^{\Delta M}$ animals. 18 hours thereafter draining lymph nodes were removed. Single cell suspensions were analyzed by flow cytometry and specific killing was calculated as [1-(% CFSE^{high} / % CFSE^{low})] x 100.

In order to obtain peritoneal macrophages, STAT3^{wt} and STAT3$^{\Delta M}$ mice were i.p. injected with 4% thioglycerol (Sigma) and sacrificed after 4h. Peritoneal macrophages were isolated by FACS analysis using antibodies against F4/80.

All mouse experiments were performed in accordance with Austrian and European laws and with the general regulations specified by the Good Science Practices guidelines of the Medical University of Vienna.

In vitro cytotoxicity assay of NK cells

STAT3^{wt} and STAT3$^{\Delta M}$ mice were injected i.p. with PBS or 100µg poly(I:C) in order to activate NK cells and spleen cells were isolated after 18 hours. Splenocytes were incubated with 5×10^4 CFSE-stained (2.5µM) YAC-1 target cells at effector-to-target ratios of 100:1, 50:1 and 25:1 in triplicates in 96-well plates. To assess the extent of spontaneously occurring apoptosis, tumor cells were incubated in the absence of NK cells. After 6h 7-AAD Viability Solution was added and cytotoxicity was quantified by flow cytometry. Cytotoxicity was normalized to quantified NK numbers of splenic single cell suspensions.

Differentiation of monocytes from primary bone marrow cells

Monocytes were differentiated from bone marrow of STAT3^{wt} and STAT3$^{\Delta M}$ mice using DMEM (Sigma-Aldrich) supplemented with Penicillin/Streptomycin (PAA), Glutamin (PAA), 10% FCS (PAA), and 10% supernatant from L-929 cells. Bone marrow cells were differentiated for 10 days and medium was changed every 2-3 days. Differentiation into monocytes was confirmed using flow cytometry.

Isolation of lamina propria lymphocytes

Lamina propria lymphocytes were isolated as described[51]. Colons of 3 mice per genotype were flushed with PBS and opened longitudinally. Tissue pieces of 3-4mm were shaken in Hank's balanced salt solution containing 5mM EDTA and 10mM Hepes at 37°C for 2x15min to separate the lamina propria lymphocytes from the epithelial layer. Then, tissue pieces were shaken in Hank's balanced salt solution containing FCS, Dispase [1U/ml], Collagenase [25U/ml] and DNAse [30U/ml] at 37°C for 3x20min. The supernatant was centrifuged and subjected to Percoll gradient centrifugation. The lymphocytes at the interface between the 40% and the 80% layers were collected, washed in ice cold PBS and then used for flow cytometry.

Histology and immunohistochemistry (IHC)

Whole intestines were flushed with PBS and 4% buffered formaldehyde and fixed as Swiss roles in 4% formaldehyde. 4μm paraffin sections representing the whole intestine were stained with H&E, alcian blue, neutrophilic esterase, toluidin blue or IHC using standard procedures. IHC stainings were performed with antibodies for Tyr-705 phosphorylated STAT3 (Cell signaling), STAT3 (Santa Cruz), Tyr-701-phoshorylated STAT1 (Cell signaling), STAT1 (Santa Cruz), Ki67 (Novocastra), cleaved caspase 3 (Cell signaling), ß-Catenin (BD Transduction Laboratories), Lysozyme (Dako), Synaptophysin (Genetex), van Willebrand Factor (DAKO), Fsp1 (Millipore), PDGFR (cell signaling), CD3 (Neomarkers), F4/80 (AbD Serotec), GranzymeB (Abcam), CD8a (Biolegend), FoxP3 (Santa Cruz), RORgT (Biolegend), CD11c (Biolegend), NKp46 (Biolegend), NKG2D (Santa Cruz), NKG2A (Biolegend), Gr1 (Serotec), Arg1 (Santa Cruz), iNOS (Biolegend), TGFß (Santa Cruz), P-SMAD2 (Chemicon), Smad7 (Santa Cruz), and detected them with peroxidase-coupled secondary antibody (ID labs) using AEC chromogen (ID labs).

Flow cytometric analysis

Spleens from STAT3^{wt} and STAT3$^{\Delta M}$ animals were squeezed through a 70μm cell strainer and red blood cells were removed using Red blood cell Lysis Buffer (Sigma) according to

manufacturer´s instruction. Splenocytes were analyzed with the following antibodies: aCD3e-Pacific Blue, aCD49b-APC-Cy7, aNK1.1-PE-Cy7, aNKp46-APC, aCD27-PE, aCD11b-PerCP-Cy5.5, aNKp46-PE, aKLRG1-FITC, aCD226-APC, Ly49A/D purified, a-Rat IgG-FITC, aLy49C/I-Biotin, Streptavidin-PerCP-Cy5.5, aNKG2D-APC, aNKG2A/C/E-FITC and aCD16/CD32 as Fc receptor block (all eBioscience). The Cell Trace CFSE Cell Proliferation Kit (Invitrogen) and the 7-AAD Viability Solution (eBioscience) was used according to the manufacturer's instruction. Samples were analyzed using a FACSCanto™ II flow cytometer (BD Biosciences) and data were calculated with FACSDiva software (BD Biosciences).

For staining of macrophages, splenic immune cells and lamina propria lymphocytes, cells were preincubated with PBS containing 0.5% BSA and FCγIII/IIR antibody to block nonspecific binding. Cells were stained with following antibodies: aCD3-Percp, aCD4-PE, aCD8-APC, aCD25-APC, aGr1-PE, aCD11c-Brilliant Violett, aCD11b-Alexa Fluor 488, aNKG2D-APC, aCD49b-PE/cy7, aCD45/B220-Alexa Fluor 488, aI-A/I-E-PerCP, aCD80-Pacific Blue, aLy49D-Fitc, aCD69-Fitc, aCD19-PE/Cy7, aCD45-Pacific Blue (all Biolegend), aFoxP3, aRORgT, aF4/80-APC, aNKp46-FITC, aNK1.1-PE (all eBioscience). Data were collected on a FACS Fortesssa (Beckton Dickinson) and analyzed with FACSdiva software software (BD Biosciences). Fluorescent cell sorting of splenocytes was performed on a BDFACS Aria (Beckton Dickinson).

Western blot

Protein extracts from whole colon, sorted peritoneal macrophages and in vitro differentiated macrophages were analyzed by Western blot using antibodies against total STAT3 (Cell Signaling).

Quantitation and staging of tumors

TissueFaxs software (TissueGnostics GmbH) was used to scan H&E-stained swiss roles. Quantitation of tumor area and IHC stainings was performed using HistoQuest software (TissueGnostics GmbH) or ImageJ. Tumor grading was performed by a board-certified pathologist.

Polymerase Chain Reaction (PCR) Analysis

Genotyping of STAT3 was performed with primers 5'-CACCAACACATGCTATTTGTAGG-3', 5'-GCAGCAGAATACTCTACAGCT-3' and 5'-GCAGCAGAATACTCTACAGCTC-3'. The Cre transgene was detected with primers 5'-CGGTCGATGCAACGAGTGATGAGG-3' and 5'-CCAGAGACGGAAATCCATCGCTCG-3'. Real-time PCR was performed with an ABI cycler (Applied Biosystems). Relative expression levels of transcripts were calculated using the

comparative CT method and normalized for GAPDH. Primer sequences are available upon request.

Laser Capture Microdissection (LCM)

5μm paraffin sections of the intestine were placed on PEN Membrane glass slides (Alphametrix Biotech). 8 slides per mouse were used for LCM using an Arcturus Alphametrix System and tumor samples were collected in Capsure Macro LCM Caps (Alphametrix Biotech). Total RNA from tumor and stroma tissue was isolated using the RNeasy FFPE kit (Qiagen) according to the manufacturer's protocol (each RNA sample represented a pool of 2 tumors isolated from one mouse; n=3 mice per genotype).

Microarray analysis

RNA from paraffin material was labeled and hybridized to mouse whole genome GeneChip Mouse Gene 2.0ST arrays (Affymetrix) according to manufacturer's instructions. Microarray data were analyzed using Limma package of R with the parameters "mouse", "tissue type" (tumor and stroma) and "genotype" using a paired approach with "mouse" as pairing variable[58]. P values were adjusted according to Benjamini-Hochberg[59]. An adjusted P value < 0.05 was considered as significant.

Weighted Gene Co-expression Network Analysis (WGCNA)

The Pearson correlations were calculated for all pairs of genes in the samples. The resulting correlation matrix was transformed into a matrix of connection strengths by raising the absolute value of the correlation coefficients to the power β. A β of 6 was used to satisfy the scale free topology criterion[54]. The top 25% of genes displaying the highest variability over the entire dataset were selected for module detection. From these genes, modules were determined using the "blockweise" module detection function of the WGCNA package with default values except for the minimal module size and the merge cut height parameters (set to 20 and 0.05 respectively). Biological functions of the single modules were determined using the GO term enrichment analysis function of WGCNA. Only "biological function" ontology was included into the analysis[55-57]. P values of enriched terms were adjusted as above according to Benjamini-Hochberg. An adjusted P value < 0.05 was considered as significant.

Statistics

Significant differences in tumor parameters, IHC stainings and RT-PCR data were calculated with GraphPad Prism 5 software using unpaired t test and Mann-Whitney post test. Multiple

comparisons were calculated with One-way Anova and Bonferroni post-test. Significant differences between experimental groups were: *P < 0.05, **P < 0.01, or ***P < 0.005.

References

1.   Markowitz SD, Bertagnolli MM. Molecular origins of cancer: Molecular basis of colorectal cancer. N Engl J Med 2009;361:2449-60.
2.   Terzic J, Grivennikov S, Karin E, et al. Inflammation and colon cancer. Gastroenterology 2010;138:2101-2114 e5.
3.   Fan Y, Mao R, Yang J. NF-kappaB and STAT3 signaling pathways collaboratively link inflammation to cancer. Protein Cell 2013;4:176-85.
4.   Quail DF, Joyce JA. Microenvironmental regulation of tumor progression and metastasis. Nat Med 2013;19:1423-37.
5.   Biswas SK, Allavena P, Mantovani A. Tumor-associated macrophages: functional diversity, clinical significance, and open questions. Semin Immunopathol 2013;35:585-600.
6.   Biswas SK, Mantovani A. Macrophage plasticity and interaction with lymphocyte subsets: cancer as a paradigm. Nat Immunol 2010;11:889-96.
7.   Pyonteck SM, Akkari L, Schuhmacher AJ, et al. CSF-1R inhibition alters macrophage polarization and blocks glioma progression. Nat Med 2013;19:1264-72.
8.   Franklin RA, Liao W, Sarkar A, et al. The cellular and molecular origin of tumor-associated macrophages. Science 2014;344:921-5.
9.   Murray PJ. The JAK-STAT signaling pathway: input and output integration. J Immunol 2007;178:2623-9.
10.   Becker C, Fantini MC, Schramm C, et al. TGF-beta suppresses tumor progression in colon cancer by inhibition of IL-6 trans-signaling. Immunity 2004;21:491-501.
11.   Bollrath J, Phesse TJ, von Burstin VA, et al. gp130-mediated Stat3 activation in enterocytes regulates cell survival and cell-cycle progression during colitis-associated tumorigenesis. Cancer Cell 2009;15:91-102.
12.   Grivennikov S, Karin E, Terzic J, et al. IL-6 and Stat3 are required for survival of intestinal epithelial cells and development of colitis-associated cancer. Cancer Cell 2009;15:103-13.
13.   Rigby RJ, Simmons JG, Greenhalgh CJ, et al. Suppressor of cytokine signaling 3 (SOCS3) limits damage-induced crypt hyper-proliferation and inflammation-associated tumorigenesis in the colon. Oncogene 2007;26:4833-41.
14.   de Jong PR, Mo JH, Harris AR, et al. STAT3: An Anti-Invasive Factor in Colorectal Cancer? Cancers (Basel) 2014;6:1394-407.
15.   Lee J, Kim JC, Lee SE, et al. Signal transducer and activator of transcription 3 (STAT3) protein suppresses adenoma-to-carcinoma transition in Apcmin/+ mice via regulation of Snail-1 (SNAI) protein stability. J Biol Chem 2012;287:18182-9.
16.   Musteanu M, Blaas L, Mair M, et al. Stat3 is a negative regulator of intestinal tumor progression in Apc(Min) mice. Gastroenterology 2010;138:1003-11 e1-5.
17.   Klampfer L. The role of signal transducers and activators of transcription in colon cancer. Front Biosci 2008;13:2888-99.
18.   Regis G, Pensa S, Boselli D, et al. Ups and downs: the STAT1:STAT3 seesaw of Interferon and gp130 receptor signalling. Semin Cell Dev Biol 2008;19:351-9.
19.   Kawada M, Seno H, Uenoyama Y, et al. Signal transducers and activators of transcription 3 activation is involved in nuclear accumulation of beta-catenin in colorectal cancer. Cancer Res 2006;66:2913-7.
20.   Rebe C, Vegran F, Berger H, et al. STAT3 activation: A key factor in tumor immunoescape. JAKSTAT 2013;2:e23010.
21.   Yu H, Pardoll D, Jove R. STATs in cancer inflammation and immunity: a leading role for STAT3. Nat Rev Cancer 2009;9:798-809.
22.   Huang S. Regulation of metastases by signal transducer and activator of transcription 3 signaling pathway: clinical implications. Clin Cancer Res 2007;13:1362-6.
23.   Kortylewski M, Kujawski M, Wang T, et al. Inhibiting Stat3 signaling in the hematopoietic system elicits multicomponent antitumor immunity. Nat Med 2005;11:1314-21.

24. Lee H, Pal SK, Reckamp K, et al. STAT3: a target to enhance antitumor immune response. Curr Top Microbiol Immunol 2011;344:41-59.

25. Gabrilovich DI, Ostrand-Rosenberg S, Bronte V. Coordinated regulation of myeloid cells by tumours. Nat Rev Immunol 2012;12:253-68.

26. Kortylewski M, Xin H, Kujawski M, et al. Regulation of the IL-23 and IL-12 balance by Stat3 signaling in the tumor microenvironment. Cancer Cell 2009;15:114-23.

27. Herrmann A, Kortylewski M, Kujawski M, et al. Targeting Stat3 in the myeloid compartment drastically improves the in vivo antitumor functions of adoptively transferred T cells. Cancer Res 2010;70:7455-64.

28. Kobayashi M, Kweon MN, Kuwata H, et al. Toll-like receptor-dependent production of IL-12p40 causes chronic enterocolitis in myeloid cell-specific Stat3-deficient mice. J Clin Invest 2003;111:1297-308.

29. Takeda K, Clausen BE, Kaisho T, et al. Enhanced Th1 activity and development of chronic enterocolitis in mice devoid of Stat3 in macrophages and neutrophils. Immunity 1999;10:39-49.

30. Dorfman DM, Shahsafaei A. CD69 expression correlates with expression of other markers of Th1 T cell differentiation in peripheral T cell lymphomas. Hum Pathol 2002;33:330-4.

31. Cheng F, Wang HW, Cuenca A, et al. A critical role for Stat3 signaling in immune tolerance. Immunity 2003;19:425-36.

32. Eckelhart E, Warsch W, Zebedin E, et al. A novel Ncr1-Cre mouse reveals the essential role of STAT5 for NK-cell survival and development. Blood 2011;117:1565-73.

33. Galon J, Costes A, Sanchez-Cabo F, et al. Type, density, and location of immune cells within human colorectal tumors predict clinical outcome. Science 2006;313:1960-4.

34. Galon J, Angell HK, Bedognetti D, et al. The continuum of cancer immunosurveillance: prognostic, predictive, and mechanistic signatures. Immunity 2013;39:11-26.

35. Fevr T, Robine S, Louvard D, et al. Wnt/beta-catenin is essential for intestinal homeostasis and maintenance of intestinal stem cells. Mol Cell Biol 2007;27:7551-9.

36. Zheng Y, Valdez PA, Danilenko DM, et al. Interleukin-22 mediates early host defense against attaching and effacing bacterial pathogens. Nat Med 2008;14:282-9.

37. Sansom OJ, Meniel VS, Muncan V, et al. Myc deletion rescues Apc deficiency in the small intestine. Nature 2007;446:676-9.

38. Karlsson G, Liu Y, Larsson J, et al. Gene expression profiling demonstrates that TGF-beta1 signals exclusively through receptor complexes involving Alk5 and identifies targets of TGF-beta signaling. Physiol Genomics 2005;21:396-403.

39. Phong MS, Van Horn RD, Li S, et al. p38 mitogen-activated protein kinase promotes cell survival in response to DNA damage but is not required for the G(2) DNA damage checkpoint in human cancer cells. Mol Cell Biol 2010;30:3816-26.

40. Coussens LM, Zitvogel L, Palucka AK. Neutralizing tumor-promoting chronic inflammation: a magic bullet? Science 2013;339:286-91.

41. Melief CJ, Finn OJ. Cancer immunology. Curr Opin Immunol 2011;23:234-6.

42. Alonzi T, Newton IP, Bryce PJ, et al. Induced somatic inactivation of STAT3 in mice triggers the development of a fulminant form of enterocolitis. Cytokine 2004;26:45-56.

43. Melillo JA, Song L, Bhagat G, et al. Dendritic cell (DC)-specific targeting reveals Stat3 as a negative regulator of DC function. J Immunol 2010;184:2638-45.

44. Klose CS, Flach M, Mohle L, et al. Differentiation of type 1 ILCs from a common progenitor to all helper-like innate lymphoid cell lineages. Cell 2014;157:340-56.

45. Angell H, Galon J. From the immune contexture to the Immunoscore: the role of prognostic and predictive immune markers in cancer. Curr Opin Immunol 2013;25:261-7.

46. Kujawski M, Kortylewski M, Lee H, et al. Stat3 mediates myeloid cell-dependent tumor angiogenesis in mice. J Clin Invest 2008;118:3367-77.

47. Schreiber RD, Old LJ, Smyth MJ. Cancer immunoediting: integrating immunity's roles in cancer suppression and promotion. Science 2011;331:1565-70.

48.   Kortylewski M, Yu H. Role of Stat3 in suppressing anti-tumor immunity. Curr Opin Immunol 2008;20:228-33.

49.   Mittal D, Gubin MM, Schreiber RD, et al. New insights into cancer immunoediting and its three component phases--elimination, equilibrium and escape. Curr Opin Immunol 2014;27:16-25.

50.   See AP, Han JE, Phallen J, et al. The role of STAT3 activation in modulating the immune microenvironment of GBM. J Neurooncol 2012;110:359-68.

51.   Wei J, Barr J, Kong LY, et al. Glioblastoma cancer-initiating cells inhibit T-cell proliferation and effector responses by the signal transducers and activators of transcription 3 pathway. Mol Cancer Ther 2010;9:67-78.

52.   Albesiano E, Davis M, See AP, et al. Immunologic consequences of signal transducers and activators of transcription 3 activation in human squamous cell carcinoma. Cancer Res 2010;70:6467-76.

53.   Lee H, Deng J, Xin H, et al. A requirement of STAT3 DNA binding precludes Th-1 immunostimulatory gene expression by NF-kappaB in tumors. Cancer Res 2011;71:3772-80.

54.   Debnath B, Xu S, Neamati N. Small molecule inhibitors of signal transducer and activator of transcription 3 (Stat3) protein. J Med Chem 2012;55:6645-68.

55.   Alonzi T, Maritano D, Gorgoni B, et al. Essential role of STAT3 in the control of the acute-phase response as revealed by inducible gene inactivation [correction of activation] in the liver. Mol Cell Biol 2001;21:1621-32.

56.   Clausen BE, Burkhardt C, Reith W, et al. Conditional gene targeting in macrophages and granulocytes using LysMcre mice. Transgenic Res 1999;8:265-77.

57.   Putz EM, Prchal-Murphy M, Simma OA, et al. PI3Kdelta is essential for tumor clearance mediated by cytotoxic T lymphocytes. PLoS ONE 2012;7:e40852.

58.   Smyth GK, Michaud J, Scott HS. Use of within-array replicate spots for assessing differential expression in microarray experiments. Bioinformatics 2005;21:2067-75.

59.   Hochberg Y, Benjamini Y. More powerful procedures for multiple significance testing. Stat Med 1990;9:811-8.
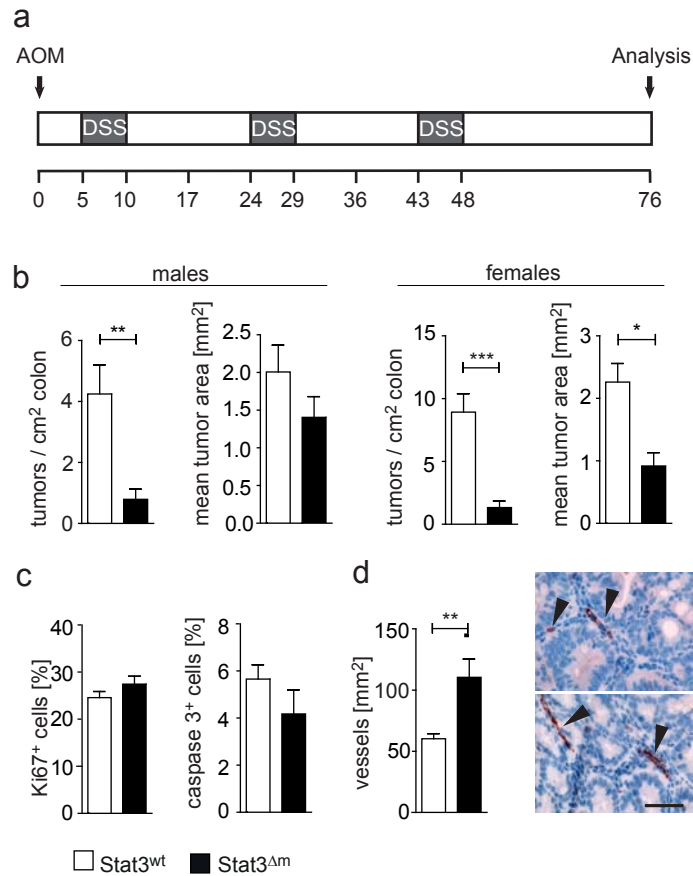
Figure 1. Myeloid STAT3 promotes formation of colorectal tumors. (a) After application of the AOM/DSS protocol (scheme), (b) Decreased colon tumor number and mean tumor size in male (n=13 for control and n=16 for STAT3$^{\Delta m}$ mice) and female (n=6 for control and n=8 for STAT3$^{\Delta m}$ mice) STAT3$^{\Delta m}$ mice. (c) Loss of STAT3 in myeloid cells had no impact on tumor cell proliferation and survival but results in (d) increased angiogenesis. Blood vessels are indicated by arrowheads. Scale bar indicates 50μm. The bar diagrams were obtained by quantitation of Ki67-positive nuclei, caspase-3-positive apoptotic cells and vWF-positive blood vessels on IHC-stained section of tumors.
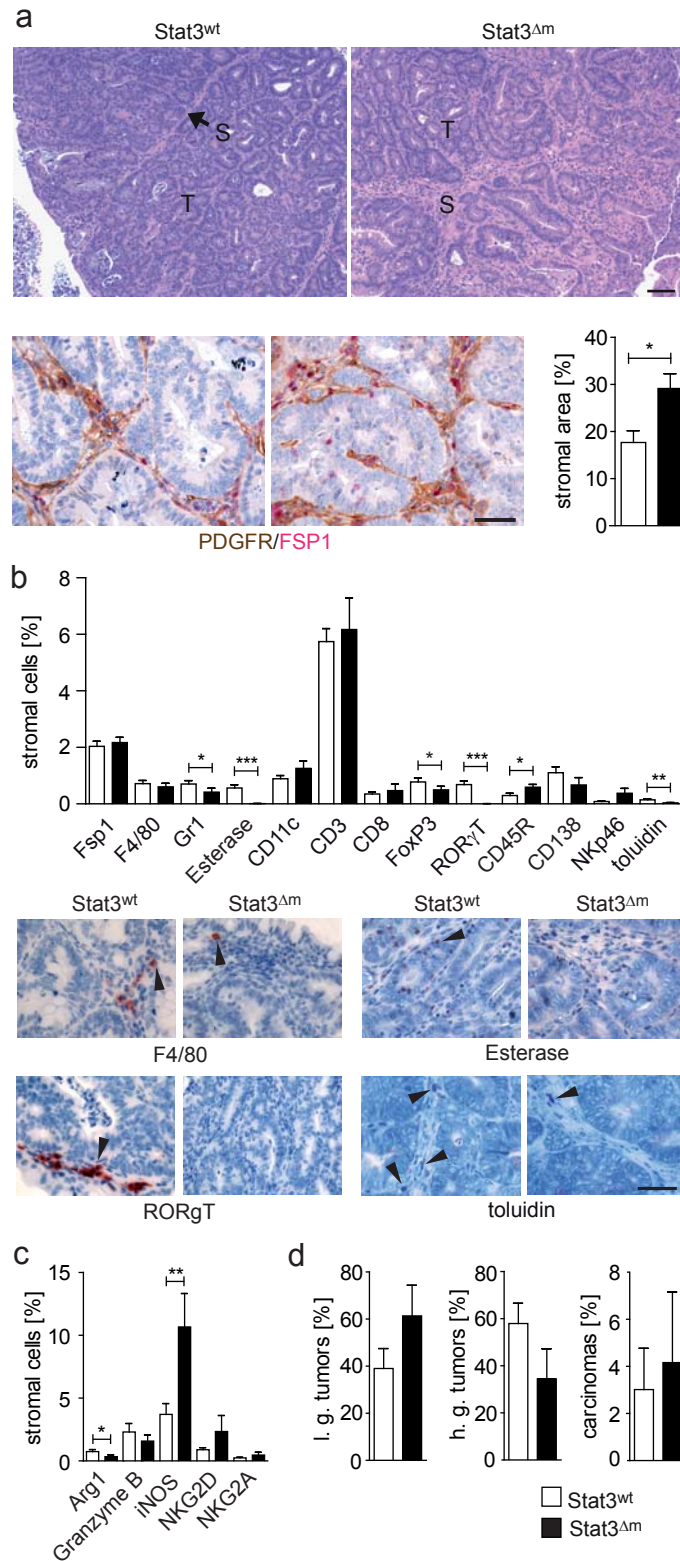
Figure 2. Loss of myeloid Stat3 changes stromal area and stromal composition of tumors. (a) Increased stromal area in Stat3^{wt} tumors: H&E staining (upper panel, scale bar indicates 100µm); Fsp1/PDGFR IHC staining (lower panel, scale bar indicates 50µm) reveals increased stromal area in Stat3$^{\Delta m}$ tumors. (b) IHC staining of stromal cells reveals similar percentage of macrophages (F4/80), reduced percentage of granulocytes (neutrophile esterase), regulatory T cells (RORgT), and Mast cells. Corresponding cell types are indicated by arrowheads. Scale bar indicates 50µm. (c) Stat3$^{\Delta m}$ tumors display reduced percentage of Arginase1$^+$ cells, and increased percentage of CD163$^+$ and iNOS$^+$ cells. IHC stainings were analysed in n≥9 tumors per mouse. (d) Histopathological grading of colon tumors in male and female mice revealed no significant change in Stat3$^{\Delta m}$ mice (calculation: number of carcinomas per mouse/total tumor number per mouse x100). 97 tumors identified in Stat3^{wt} mice and 26 tumors identified in Stat3$^{\Delta m}$ mice were analysed.
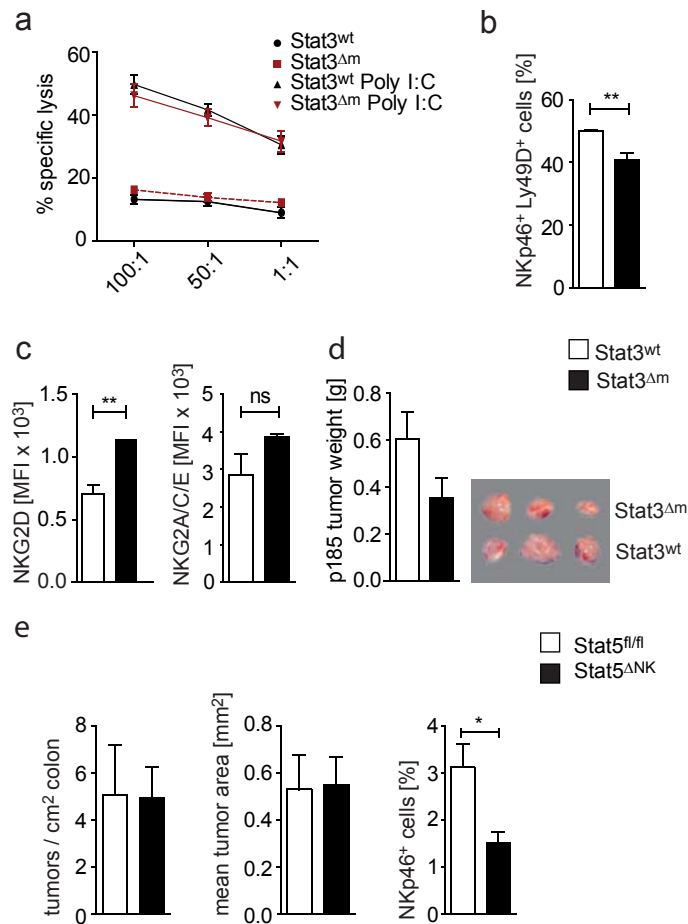
Figure 3. In vitro NK cytotoxicity assay and characterization of NK cells from spleens of Stat3$^{\Delta m}$ and control mice. (a) flow cytometric analysis of specific lysis of CFSE-labeled YAC-1 target cells in different effector:target ratios by splenocytes from Stat3$^{\Delta m}$ and control mice, injected with phosphate buffered saline or Poly(I:C) (n=3 per group). (b) Flow cytometric analysis of Stat3$^{\Delta m}$ and control splenocytes demonstrating reduced percentage of CD3$^-$ NKp46$^+$ Ly49D$^+$ cells (n≥4). (c) tumor weight of transplanted p185 tumor cells into Stat3$^{\Delta m}$ and control mice (n=15 tumors in control and n=11 tumors in Stat3$^{\Delta m}$ mice). (d) Loss of NK cells does not affect tumor initiation and tumor growth in long term AOM/DSS treated Stat5$^{\Delta NK}$ mice. (e) Analysis of tumor multiplicity (tumors/cm^2 gut) and tumor size (mean tumor area) revealed similar tumor numbers and tumor size upon loss of NK cells (n=11 for Stat5$^{\Delta NK}$ mice and n=8 for Stat5$^{fl/fl}$); flow cytometric analysis reveals reduced colon NK (CD45$^+$ CD3$^-$ CD19$^-$ NKp46$^+$) cells.
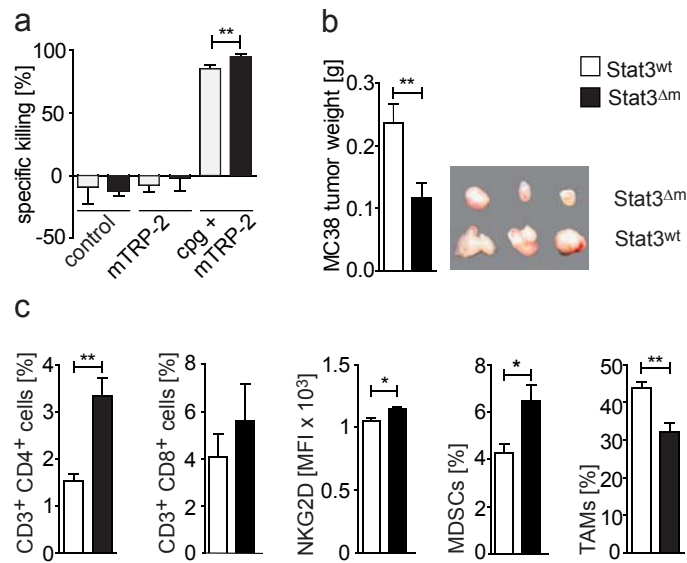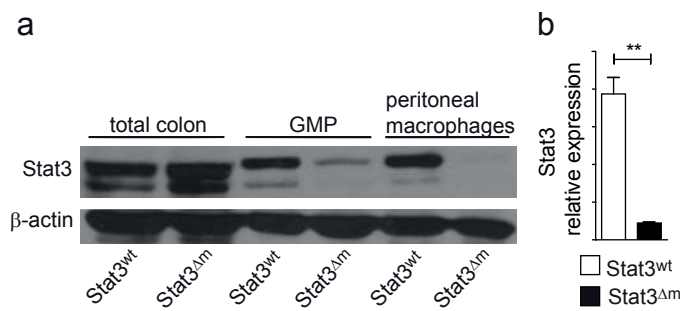
Figure 4. Characterization of cytotoxic T lymphocytes in Stat3$^{\Delta m}$ mice. (a) In vivo cytotoxicity assay of Stat3$^{\Delta m}$ and control mice immunized with 0.1mg/mouse m-TRP2$_{181\text{-}188}$ in combination with the adjuvant CpG-ODN 1668. Specific killing ([1-(% CFSE^{high} / % CFSE^{low})] x 100) was calculated of CFSE-labeled target cells analysed via flow cytometry (n=x per group). (b) tumor weight of transplanted MC38 tumor cells into Stat3$^{\Delta m}$ and control mice (n=12 tumors in control and n=14 tumors in Stat3$^{\Delta m}$ mice); flow cytometric analysis of MC38 tumors reveals increased numbers of NKG2D$^+$ cells, increased percentage of T cells, MDSCs (Gr1^{hi} CD11b$^+$ cells) and TAMs (Gr1^{lo} CD11b$^+$ CD11c^{lo}) cells.
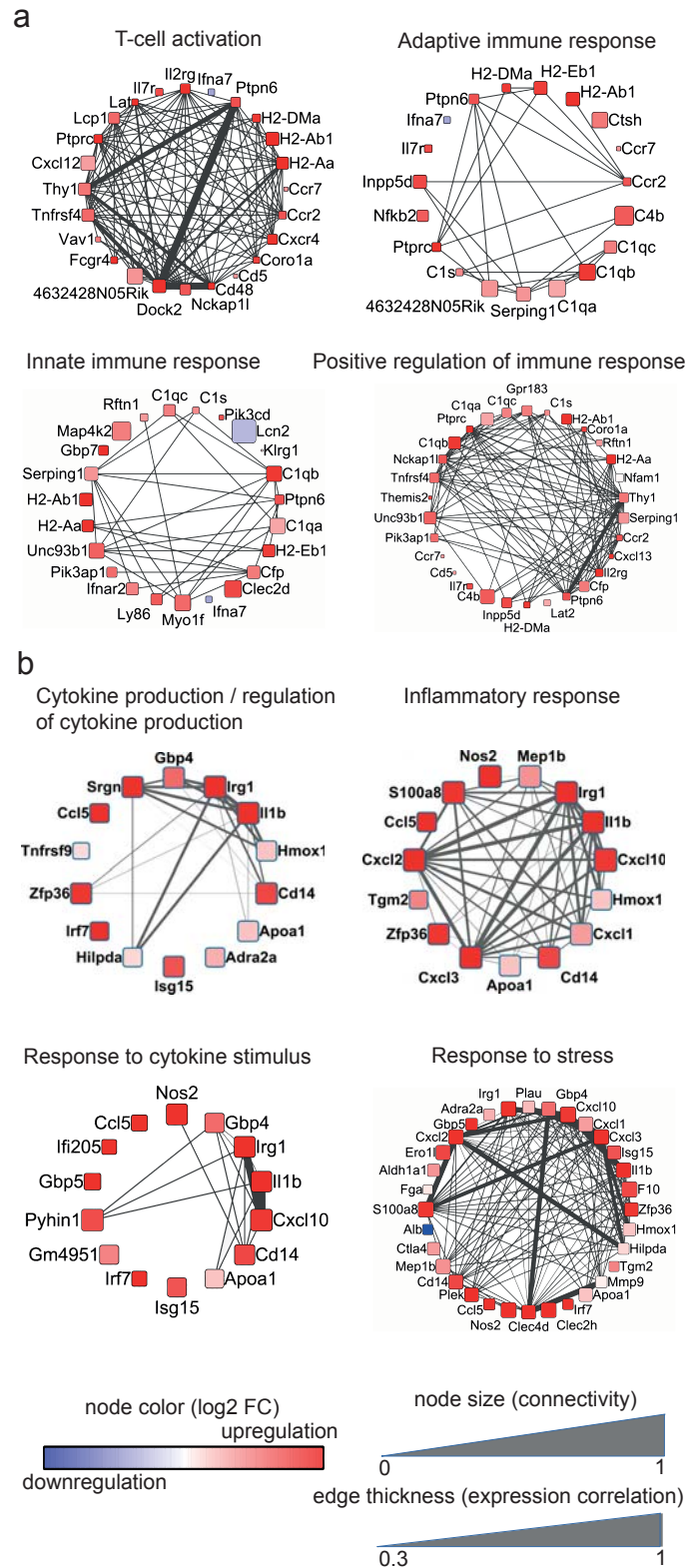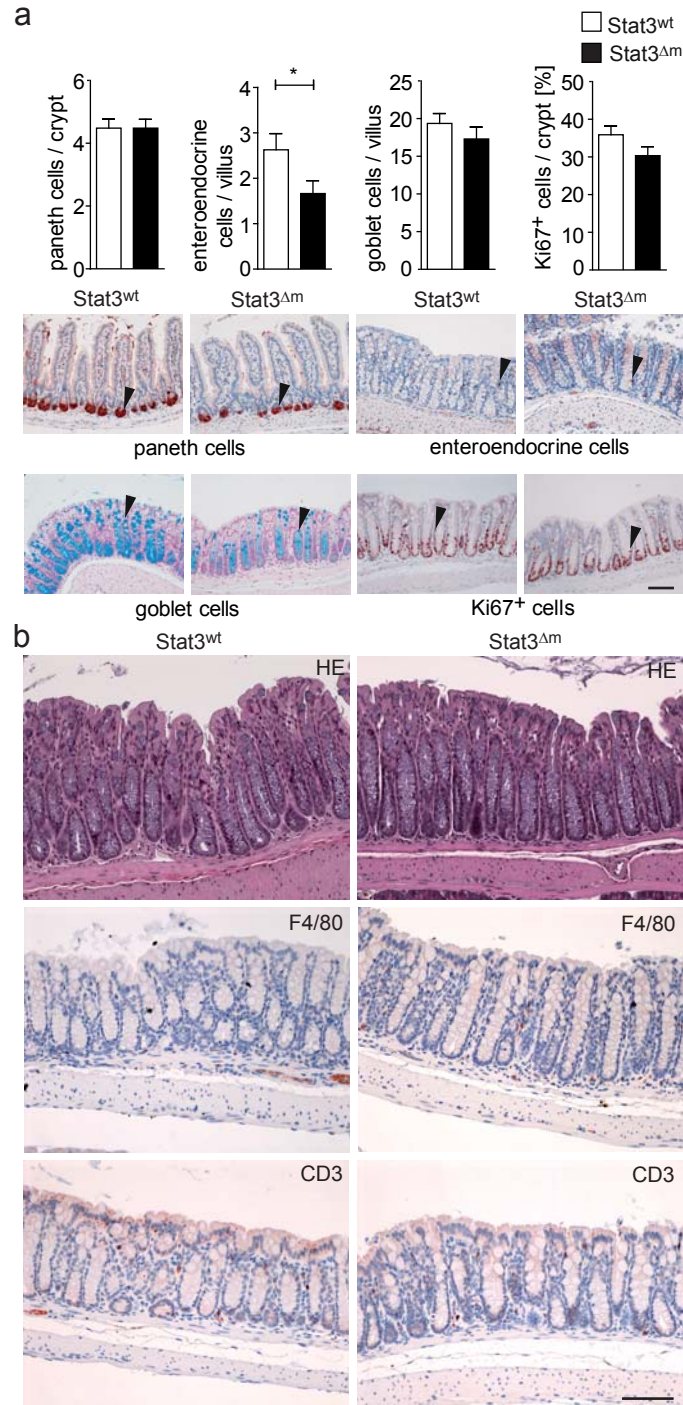
Figure 5. Weighted Gene Co-expression Network Analysis of microarray data obtained from RNA of laser-capture-microdissected colorectal tumors from Stat3$^{\Delta m}$ and control tumors. Gene expression was compared between Stat3$^{\Delta m}$ stroma and Stat3^{wt} stroma. Modules of highly correlated genes were identified for (a) Immune response genes, and (b) Inflammatory response genes. Blue node color represents downregulation, red node color represents upregulation of gene expression in the stroma of Stat3$^{\Delta m}$ tumors. Node size is associated with the gene's co-expression in the entire dataset; edge (line) thickness is linked to the gene's connectivity (co-expression within the module).
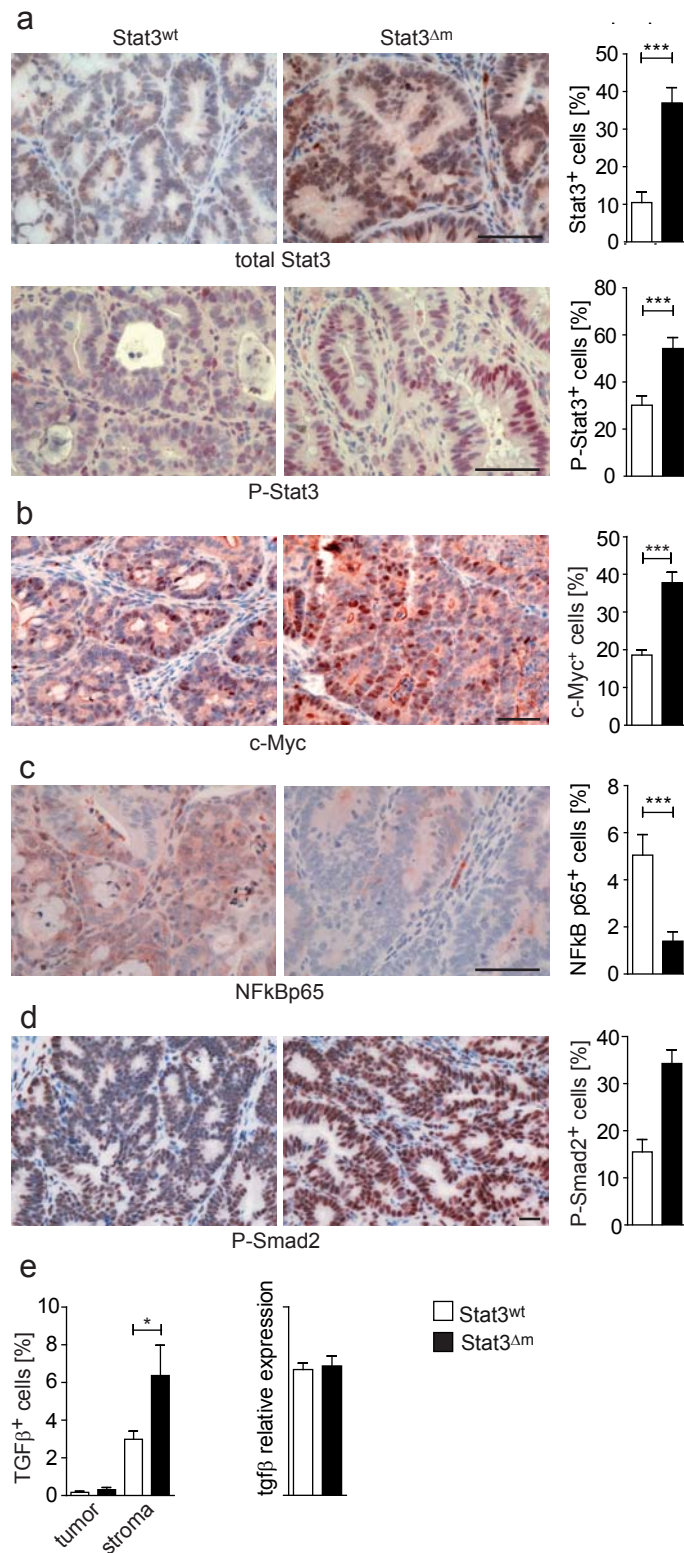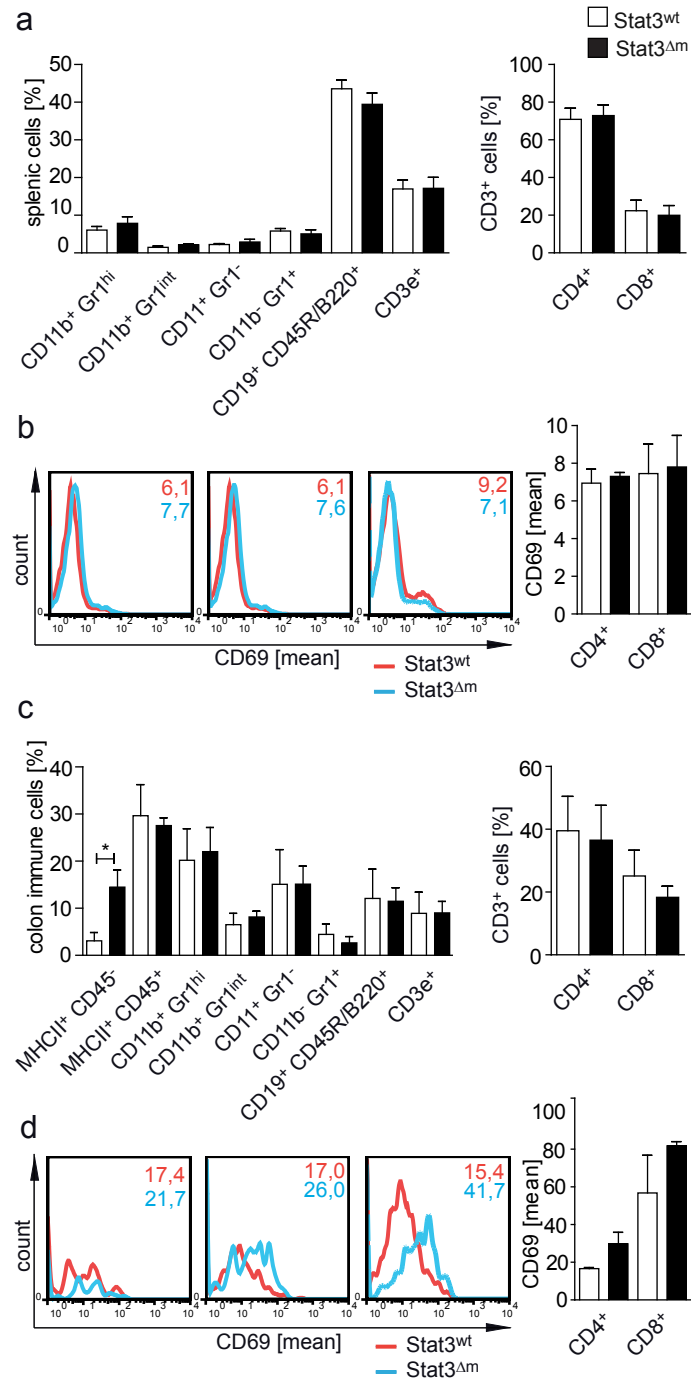
Figure 6. Immunohistochemistry stainings of colon tumors in long term AOM/DSS treated Stat3wt and Stat3Δm mice (n≥9 tumors per genotype). (a) IHC staining for total Stat3 and Tyr-705-phosphorylated Stat3 (P-Stat3) revealed higher levels in Stat3Δm tumors compared to Stat3wt. (b) c-Myc IHC staining demonstrated increased expression in Stat3Δm tumors. (c) IHC staining for NFkB p65 revealed reduced number of positive tumor cells in Stat3Δm tumors. (d) P-Samd2 IHC demonstrated increased numbers of positive cells in Stat3Δm tumors. (e) IHC staining for TGFβ revealed higher levels of positive cells in the stroma but not tumor cells of Stat3Δm tumors; IHC stainings were analysed in n≥9 tumors per genotype. Real-time polymerase chain reaction analysis demonstrates similar tgfβ levels in bone marrow – derived macrophages of Stat3wt and Stat3Δm mice (bars represent data +/- standard error of mean from 3 animals per genotype). Scale bar indicates 50µm.

a

	total colon	GMP	peritoneal macrophages

Stat3

β-actin

Stat3^{wt} Stat3^{Δm} Stat3^{wt} Stat3^{Δm} Stat3^{wt} Stat3^{Δm}

b

**

Stat3 relative expression
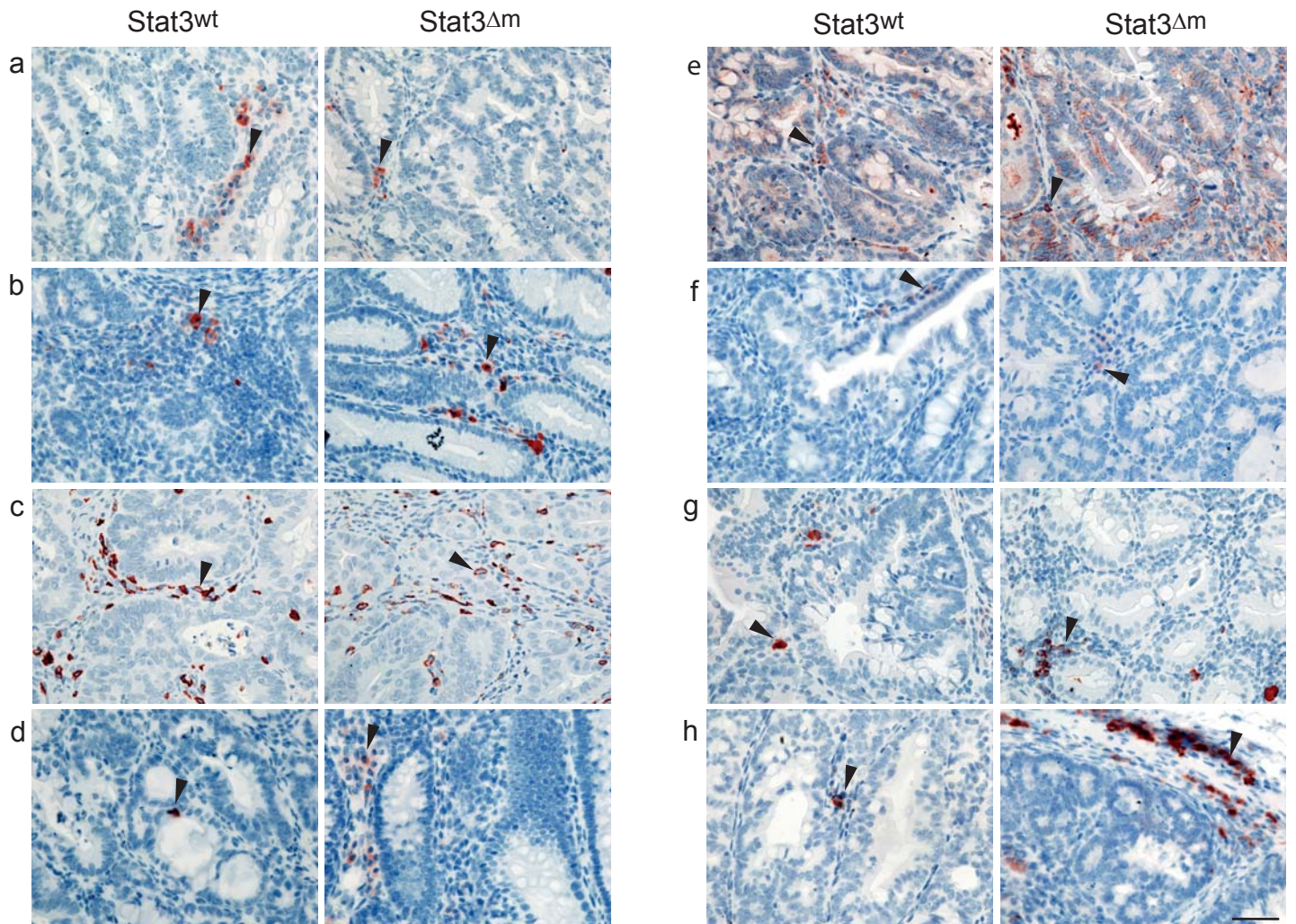
☐ Stat3^{wt}
■ Stat3^{Δm}

Supplementary Figure 1. Confirmation of Stat3 ablation in myeloid cells. (a) Western blot analysis for total Stat3 demonstrating loss of Stat3 protein in tissue from total colon (n=3 mice per genotype), granulocyte-monocyte progenitors derived from bone marrow (FACS blot, n=3 mice per genotype) and peritoneal macrophages (n=3 mice per genotype) in Stat3^{Δm} mice. GAPDH was used as loading control. (b) Real-time polymerase chain reaction analysis of Stat3 in macrophages FACS-sorted from splenocytes of Stat3^{wt} and Stat3^{Δm} mice. Bars represent data +- standard error of mean from 6 animals per genotype.

Supplementary Figure 2. Characterization of mice with a conditional ablation of Stat3 in myeloid cells. (a) Quantitation of paneth cells, enteroendocrine cells and goblet cells in the colon of Stat3$^{\Delta m}$ mice. The bars represent average numbers of positively stained cells +- standard error of mean in 9 crypts or villi (n=3 mice per genotype). Immunohistochemistry for Lysozyme and Synaptophysin, and Alcian blue-staining demonstrated the presence of paneth cells, enteroendocrine cells, and goblet cells in the colon of Stat3$^{\Delta m}$ mice. Ki67-staining revealed proliferating cells in the crypts of Stat3$^{\Delta m}$ mice. Corresponding cell types are indicated by arrowheads. (b) H&E staining and Immunohistochemistry staining for F4/80 and CD3 of colons from untreated Stat3$^{\Delta m}$ and control mice. Scale bar indicates 100µm.
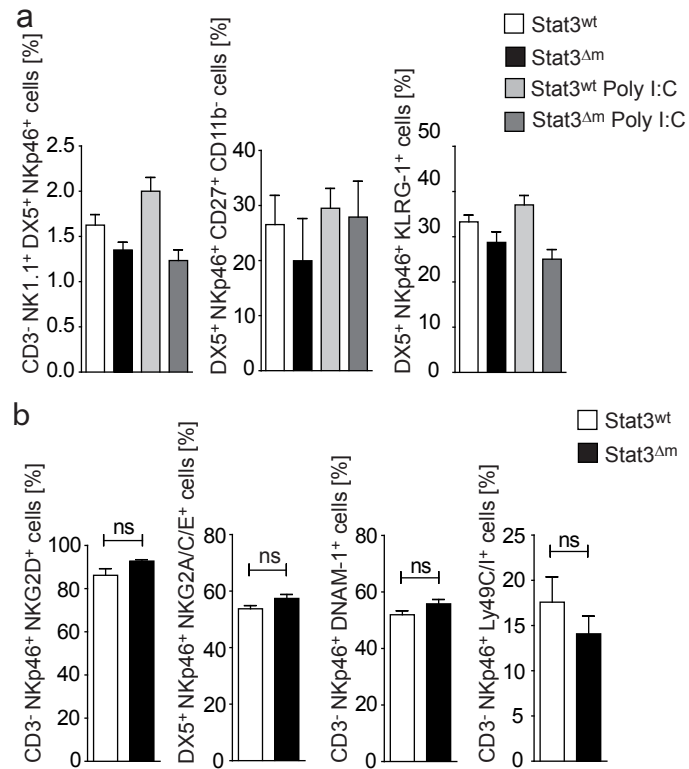
Supplementary Figure 3. Flow cytometric analysis of splenic cells and lamina propria immune cells after short term DSS treatment in Stat3wt and Stat3Δm mice. (a) splenic immune cells, (b) similar levels of CD3+ CD4+ cell activation; (c) lamina propria immune cells, (d) increased CD3+ CD4+ cell activation.

Supplementary Figure 4: Charakterization of stromal composition of Stat3wt and Stat3Δm tumors. Immunohistochemistry stainings for (a) granulocytes (Gr1), (b) dendritic cells (CD11c), (c) T cells (CD3) , (d) cytotoxic T cells (CD8), (e) Plasma cells (CD138), (f) regulatory T cells (FoxP3), (g) B cells CD45R, (h) NK cells (NKp46) of Stat3wt and Stat3Δm colon tumors; n≥9 tumors per genotype. Corresponding cell types are indicated by arrowheads. Scale bar indicates 50μm.

Supplementary Figure 5. Flow cytometric analysis of splenic NK cells. (a) Similar expression of Dx5 and maturation markers (CD27, KLRG-1) in Stat3$^{\Delta m}$ and control mice (n=3 mice per group). (b) Similar expression of NKG2D, NKG2A and Ly49C/I in Stat3$^{\Delta m}$ and control mice (n≥4).
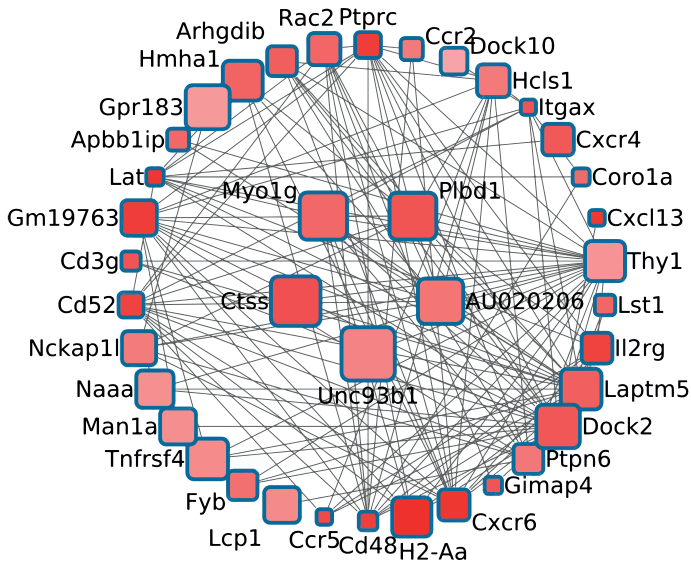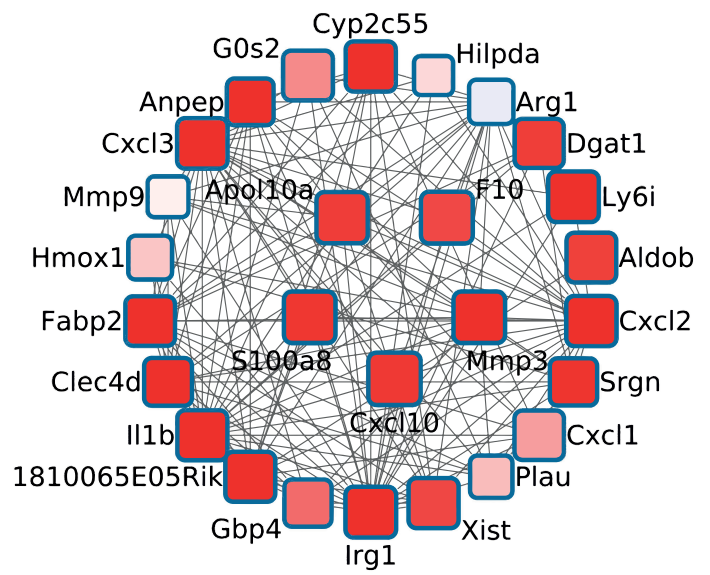
Term ID	Term Name	p value
GO:0002684	positive regulation of immune system process	4,25E-10
GO:0002682	regulation of immune system process	8,74E-10
GO:0002443	leukocyte mediated immunity	2,04E-08
GO:0042110	T cell activation	2,32E-08
GO:0050778	positive regulation of immune response	1,02E-06
GO:0002250	adaptive immune response	1,73E-06
GO:0051251	positive regulation of lymphocyte activation	2,12E-06
GO:0045087	innate immune response	1,13E-05
GO:0002696	positive regulation of leukocyte activation	1,32E-05
GO:0019724	B cell mediated immunity	2,02E-05
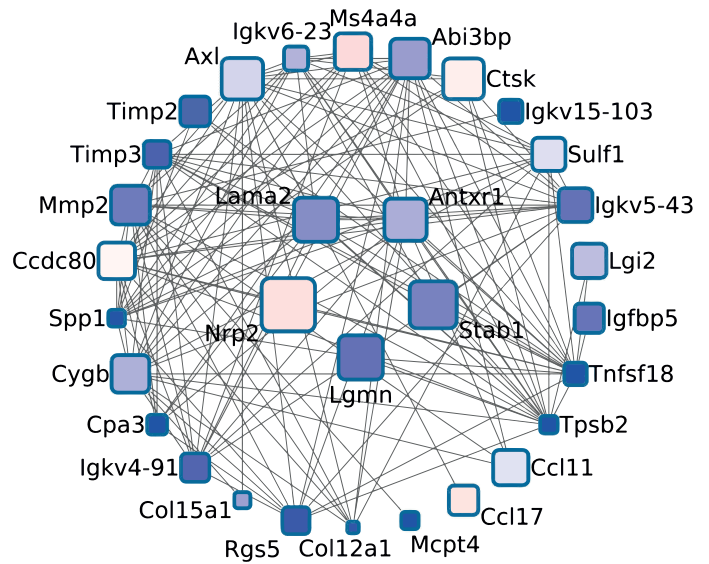
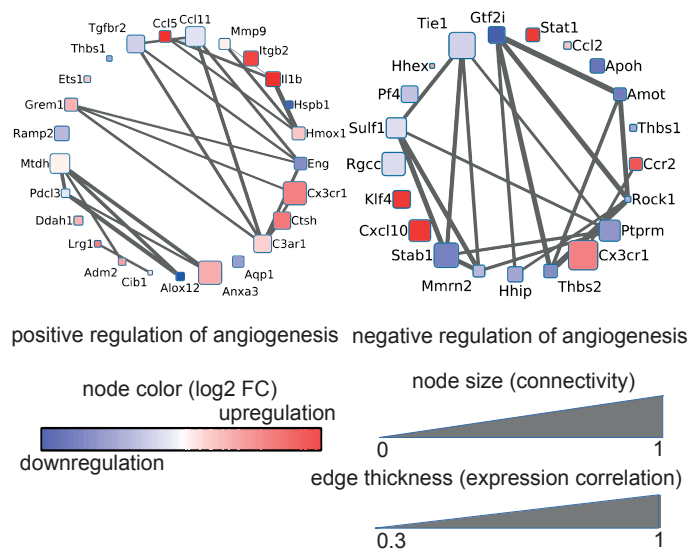| Term ID	Term Name	p value
GO:0001944	vasculature development	1,94E-07
GO:0030334	regulation of cell migration	2,83E-07
GO:2000145	regulation of cell motility	3,52E-07
GO:0001568	blood vessel development	5,38E-07
GO:0016477	cell migration	1,18E-06
GO:0048514	blood vessel morphogenesis	1,62E-05
GO:0001525	angiogenesis	3,93E-05
GO:0072358	cardiovascular system development	7,73E-05
GO:0072359	circulatory system development	7,73E-05
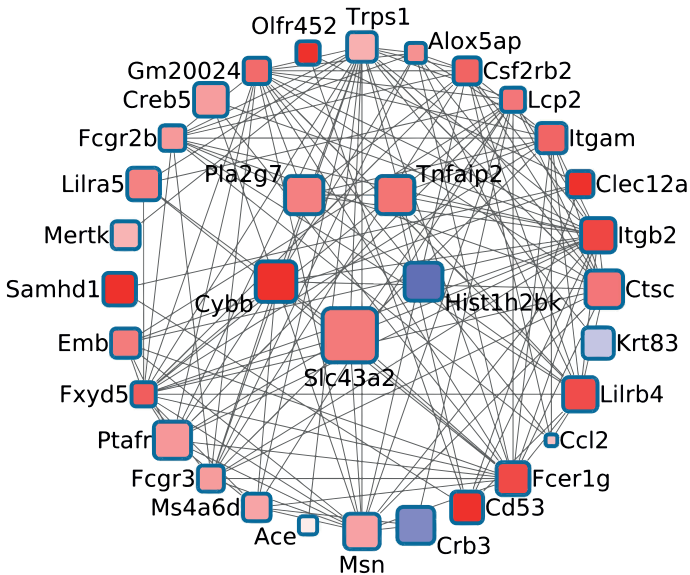
| Term ID	Term Name	p value
GO:0002376	immune system process	8,77E-04
GO:0030593	neutrophil chemotaxis	1,17E-03
GO:0050900	leukocyte migration	1,80E-03
GO:0030595	leukocyte chemotaxis	3,04E-03
GO:0050766	positive regulation of phagocytosis	4,69E-03
GO:0060326	cell chemotaxis	1,13E-02
GO:0050764	regulation of phagocytosis	1,54E-02
GO:0002438	acute inflammatory response to antigenic stimulus	9,28E-02

| Term ID	Term Name	p value
GO:0001817	regulation of cytokine production	2,34E-03
GO:0009611	response to wounding	2,55E-03
GO:0048878	chemical homeostasis	1,15E-02
GO:0001816	cytokine production	2,50E-02
GO:0006954	inflammatory response	2,98E-02
GO:0006952	defense response	7,34E-02

Supplementary Figure 6. The Cytoscape plots and significantly enriched GO terms. The four most enriched terms or signaling pathways in knockout vs wildtype modules are shown representing the top 150 protein connections in each color module as calculated by adjacency between genes. Node size represents connectivity and the nodes in the middle of each Cytoscape plot are the "hub genes" for each module.

positive regulation of angiogenesis   negative regulation of angiogenesis

node color (log2 FC)
upregulation
downregulation

node size (connectivity)
0   1

edge thickness (expression correlation)
0.3   1

Supplementary Figure 7. WGCA of microarray data from laser-capture-microdissected colorectal tumors, comparing Stat3$^{\Delta m}$ stroma and Stat3^{wt} stroma for the module "angiogenesis".
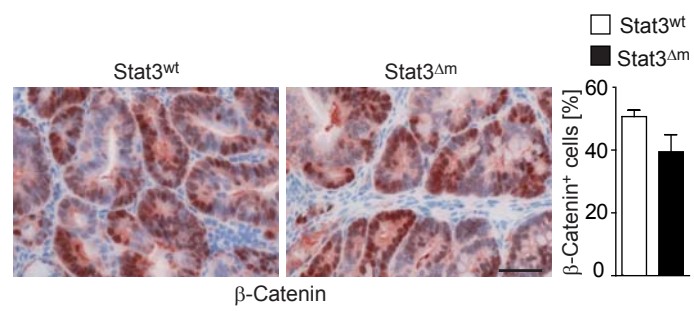
Supplementary Figure 8. β-Catenin levels are similar between Stat3^{wt} tumors and Stat3$^{\Delta m}$ tumors. Scale bar indicates 50μm.
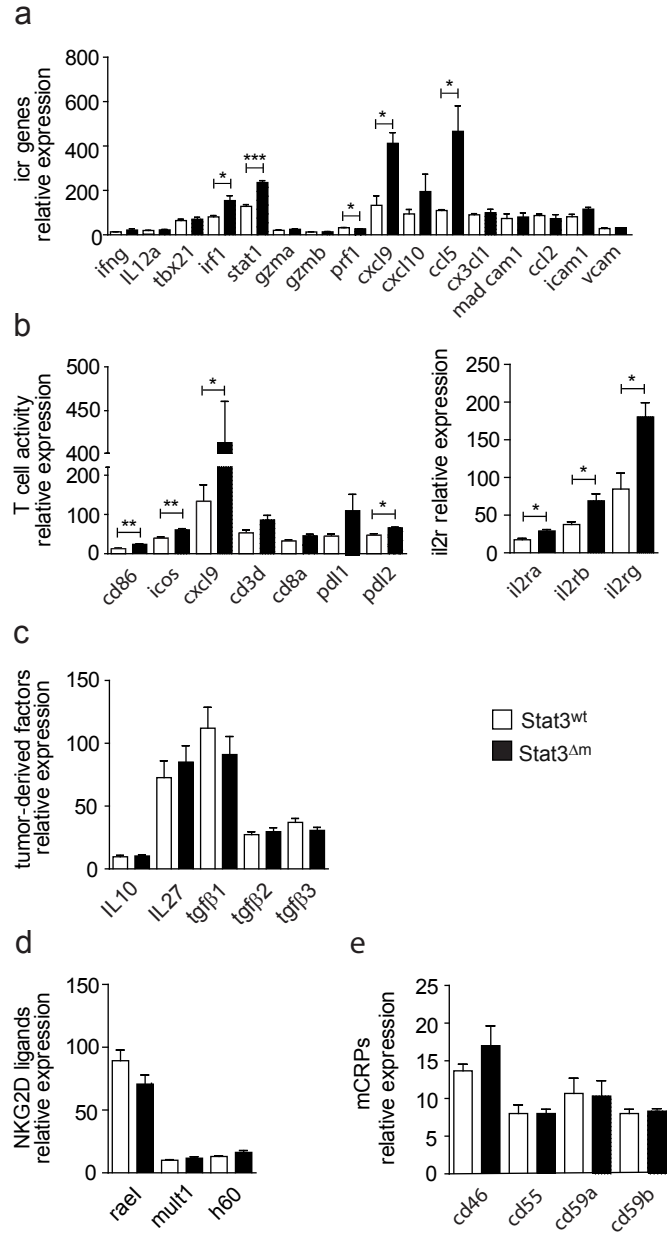
Supplementary Figure 9. RNA expression data of laser-capture microdissected tumor and stroma tissue from Stat3$^{\Delta m}$ and control mice. (a) ICR (Immunologic Constant of Rejection) genes (b) T cell activity (left panel), IL-2 receptors (right panel), (c) tumor-derived factors(left panel), (d) stress-induced NKG2D ligands (e) mCRPs.